Granular Matter (2016) 18:1
DOI 10.1007/s10035-015-0597-6

ORIGINAL PAPER

Numerical and experimental verification of a damping model used in DEM

Wei Zhou[1] · **Xing Ma**[1] · **Tang-Tat Ng**[2] · **Gang Ma**[1] · **Shao-Lin Li**[1]

Received: 20 March 2015 / Published online: 21 January 2016

Abstract This paper presents a study on the damping ratio (β) used in discrete element simulations. Physical experiments are performed by dropping particles from a predetermined height. Two kinds of granular particles, aluminum and steel spheres, are used. The size of these particles are the same. The process of particle depositing under gravity is simulated using the discrete element method. The experimental observation is compared with the numerical result to identify the appropriate β. The result indicates that the appropriate damping ratio used in discrete element simulations is between 0.2 and 0.3 %. Various β are then used in the numerical simulations to study the effect of β on the dropping process. The final height of the sample relates to β and the drop height. The effect of β is more profound for small drop height. For greater drop height, the effect of β is negligible.

Keywords Granular materials · Discrete element method (DEM) · Damping

1 Introduction

Discrete element method (DEM), introduced by Cundall and Strack [1], has been applied to many engineering fields especially in the area of granular materials. DEM has been shown to be a promising tool in both fundamental research and in industrial applications of particulate materials for its simplicity of the contact model and the easy interaction between particles and other boundaries. Relating the properties of granular materials to the input parameters of DEM is of great importance to resemble the physical bulk behavior of granular materials [2]. Input parameters without any justification may introduce questions on the validity of the results. Trial-and-error method is commonly used to determine the suitable microscopic variables of the DEM model to establish the similar static or dynamic behavior between the physical and numerical tests [4–6]. Input parameters of DEM such as shear modulus (stiffness), density, and damping have been investigated under zero gravitational force [3]. The result indicates that similar results can be observed when the parameters are within some ranges.

Influence of damping has also been analyzed using the restitution coefficient [7–12]. Krijt [13] provided an overview of researches on the restitution coefficient of the incident velocities of particles subjected to normal collisions. These fundamental studies are on particle collisions between two solid spheres or between a sphere and a plate. DEM simulations of more complex collisions of particles have been studied using a particle vibration damper [14,15]. Many recent studies on the energy dissipation have been focused on the friction between particles [16–18]. Study on the damping ratio has been limited.

Ng et al. [19] have found that damping can be manipulated to simulate the sample preparation at different drop heights. They suggested a damping ratio of 0.2 % for DEM simulations. But the value has not been verified by physical testing. It is useful to validate the appropriate (correct) damping range that produces similar response of physical tests. We should have more confidence on the DEM results using the correct damping.

In this paper, physical experiments and numerical simulations of sample preparation under gravity have been carried out to investigate the effect of damping. The results of numer-

✉ Wei Zhou
zw_whuedu@163.com

[1] State Key Laboratory of Water Resources and Hydropower Engineering Science, Wuhan University, Wuhan, China

[2] Civil Engineering Department, University of New Mexico, Albuquerque, NM 87131, USA

ical simulations are compared with the experimental data to determine the appropriate range of damping. Then, a parametric study on the damping and drop height is presented.

The experiment is picked for its simplicity and can be modelled by DEM with high fidelity. The system is more complicated than a binary-collision experiment because this work focuses on the damping used for particle assemblies which contain lots of particles but not for a single particle. The value of damping ratio determined here is reliable for DEM particle assemblies. But its reliability for binary collisions may need more researches.

2 Experimental tests

Experiments of dropping metal particles (aluminum and steel) from a predetermined height have been carried out to investigate the relationship between the final height of sample (h_f) and the drop height (h_0). The metal spheres are precision ball bearings. The diameter is 8.0 mm. Each sample contains 6000 spheres. The experimental results will be compared with DEM simulations.

Prior to dropping of the particles in each test, we create a similar dense assembly first. The particles are assembled in a rectangular box with an acrylic plate on top. A small seating load is placed on the plate. Then the assembly is densified by vibrating the box. The height of the assembly is measured after every 10 s of vibration. When the measured height remains unchanged, the assembly is considered to be ready. Figure 1 shows the photographs of the assemblies after densification. The height of the dense assemblies is almost the same before each drop tests (1541.5 mm for aluminum balls and 1501.0 mm for steel balls). The assembly of steel spheres is denser. This may be due to the difference in friction coefficient and density. DEM result has shown that smaller friction coefficient between particles produces denser samples in sample preparation. A smaller friction coefficient in steel balls (0.15) comparing 0.18 for aluminum balls may be the factor that denser assemblies are obtained for steel balls. In addition, the density of steel (7.85×10^3 kg/m^3) is greater than that of aluminum (2.70×10^3 kg/m^3). A greater gravitational force is applied to the steel balls during vibration.

Particles are released at three different drop heights (225, 425 and 800 mm) into a transparent square tube. Figure 2 shows the configuration before the drop (the drop height is 225 mm). Figure 3 shows the dimensions of the box and tubes. Particles drop through the trap door at the bottom of the box. The drop tests are repeated five times at each drop height to determine the final height of the assemblies. Since the surface of the final sample is not even, the final height is the average of the highest and lowest points of the surface as shown in Fig. 4. The result is presented in Fig. 5. The vertical bars represent the SD of the measured h_f. The crosses are the averages of h_f. The boxes are averages $\pm 0.5 \times$ SD. Due to the limited range of the drop height, the average height of the final sample may not be affected by the drop heights

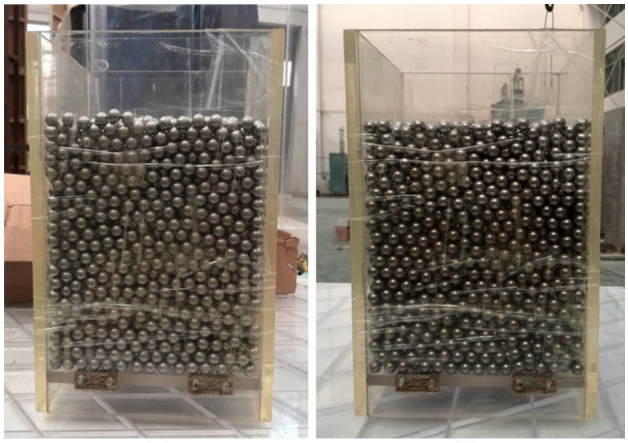

(a) (b)

Fig. 1 The assemblies after being densified. **a** Aluminum balls, **b** steel balls

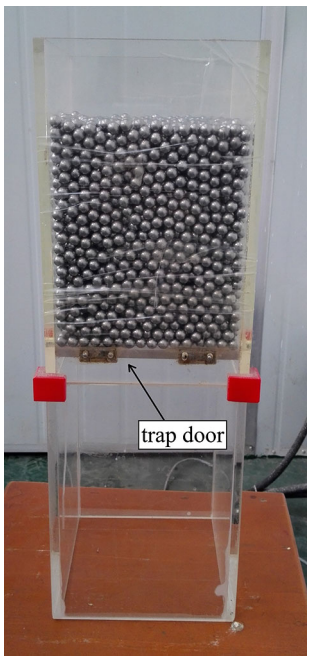

Fig. 2 The configuration at the beginning of the drop test with the drop height of 225 mm

3 Numerical simulation

The DEM program ELLIPS3H is employed here to conduct the numerical drop tests. A detailed description of the program can be found in the literature [20].

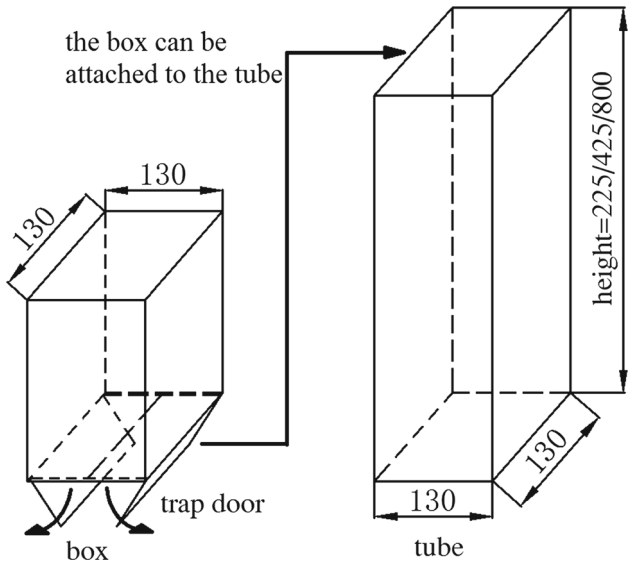

Fig. 3 The sketches of the *box* and *tubes* (unit of the lengths is mm)

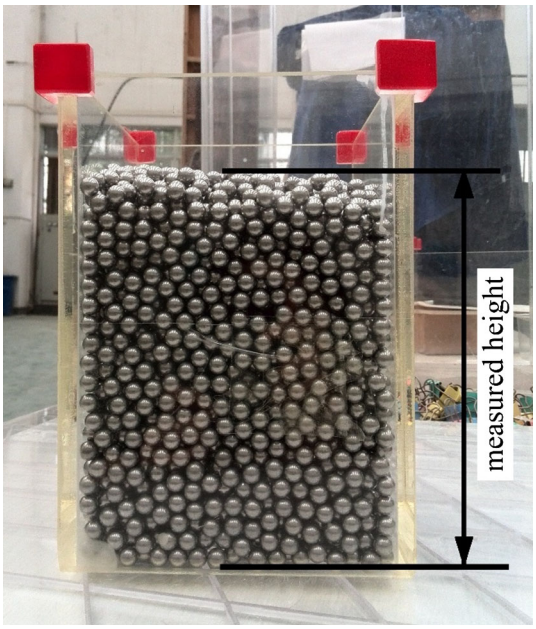

Fig. 4 Measured height of a sample after test

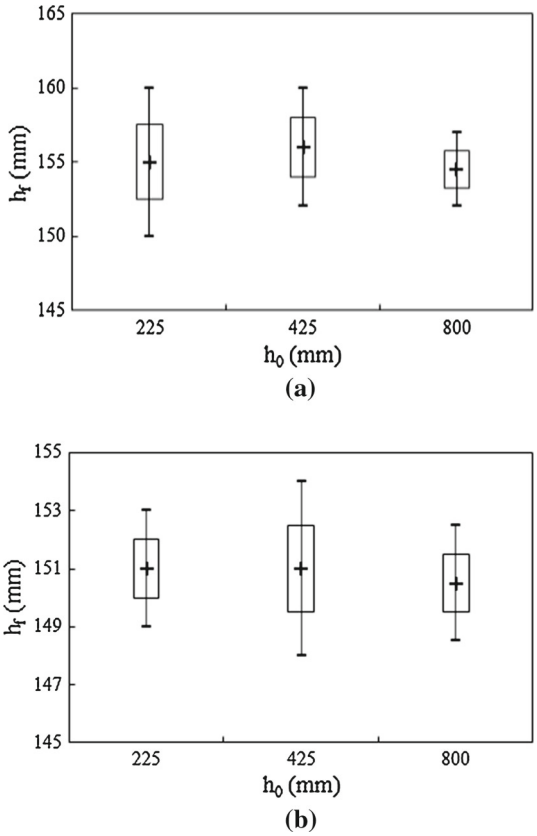

Fig. 5 The result of experimental tests. **a** Aluminum balls, **b** steel balls

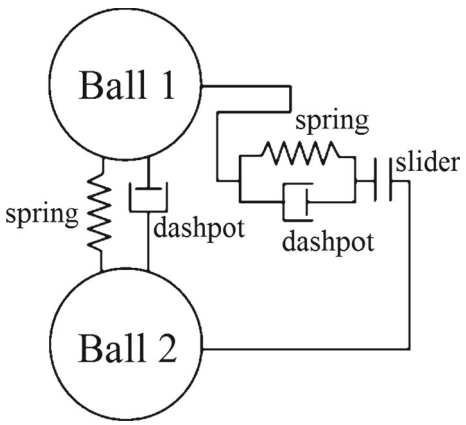

Fig. 6 Particle contact model

3.1 Contact model

A contact model describes the physical behavior occurring at a contact. A typical contact model including springs, dashpots and sliders are shown in Fig. 6 [21]. The normal spring is estimated using the Herzian model. The tangential spring is the simplified Mindlin's tangential contact law. This contact model is defined by two intrinsic parameters: shear modulus G and Poisson's ratio ν of the material of the two balls. The normal stiffness according to the Hertzian theory is given as:

$$k_n = \frac{2Ga}{1-\nu} \tag{1}$$

where G is the shear modulus, a is the equivalent radius of the contact area which is a function of the normal force, ν is the Poisson's ratio.

In the simplified Mindlin's tangential contact law, the initial tangential stiffness of the Mindlin theory is used. The relationship between the tangential stiffness and the normal stiffness is:

$$\frac{k_t}{k_n} = \frac{2(1-v)}{(2-v)} \tag{2}$$

The mass proportional damping force is used in the Program ELLIPS3H. The dashpot coefficient c is:

$$c = 2\pi\alpha m \tag{3}$$

where α is a damping input parameter, m is the particle mass. The damping ratio β can be described as:

$$\beta = \frac{c}{c_{crit}} \tag{4a}$$

$$\beta = \pi\alpha\sqrt{\frac{m}{k}} \tag{4b}$$

where k is the largest stiffness at the contact between particles, c_{crit} is critical damping of the system:

$$c_{crit} = 2m\omega_n \tag{5}$$

where ω_n is the natural frequency of the system. The damping ratio β is specified in the simulations. Ng et al. [19] suggested 0.002 for β in the quasi-static simulations. Apart from the previous DEM simulations, damping is only applied when collision happens [7]. During the free fall of the particles, the damping is zero in the kinematic equation.

3.2 Sample preparation

The same diameter (8.0 mm) and total number (6000) of spheres as the physical tests are used in DEM simulations. The shear modulus and Poison's ratio of the aluminum and steel spheres are 26 GPa and 0.34, 80 GPa and 0.26, respectively. The densities of the aluminum and steel spheres (ρ) are 2.70×10^6 kg/m^3 and 7.85×10^6 kg/m^3, respectively. They are 1000 times higher than the real values of aluminum and steel. The computational effort can be reduced using this mass scaling, because a larger time step can be applied in the numerical simulations. The gravity constant is reduced to 9.81×10^{-3} m/s^2 to produce the correct unit weight (γ) of the aluminum and steel spheres (26.49 kN/m^3 and 77.01 kN/m^3).

The process of numerical sample preparation is divided into three phases. The preparation steps are shown in Fig. 7. In phase one, spheres with an artificial small radius (3 mm) are randomly generated in a rectangular prism. The dimensions of the regular prisms are different for steel and aluminum spheres. The dimensions of the regular prisms of sample of aluminum spheres (SA) and sample of steel spheres (SS) are 130:130:154 and 130:130:150 mm, respectively. The differences of the dimensions in the z-direction (154 and 150 mm) is according to the observed initial dimensions in the physical tests. Particles are then expanded until the desired radius (4 mm) is obtained. A smaller friction coefficient 0.01 and a damping ratio β of 0.002 is used in this phase. The reduced friction coefficient decreases computation effort so that a dense packing can be achieved quickly [22]. Then, the unbalanced forces are monitored till the system is in equilibrium. The unbalanced force of a particle is the resultant of all contact forces acting on the particle. Previous study indicates that the system can be considered in equilibrium when the unbalanced force ratio (the ratio of the mean unbalanced force to the mean contact force) $\leqslant 1\,\%$ [3]. Small initial stress on the top wall (0.302 kPa for SA and 0.625 kPa for SS) are

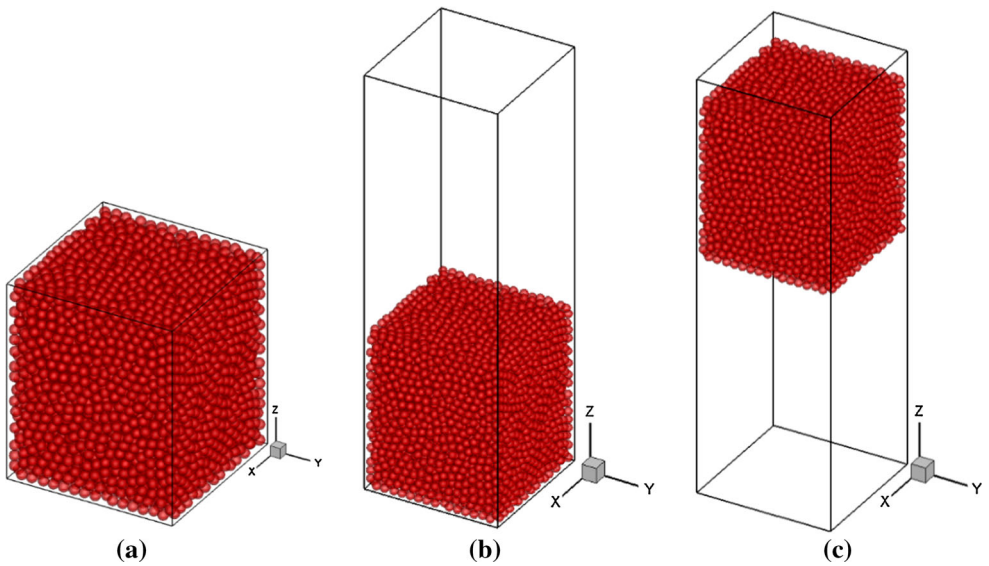

Fig. 7 Preparation of samples: **a** initial configuration of packed assembly; **b** release of residue stress and achieve equilibrium; **c** raise particles to the drop height

Table 1 Characteristics of Sample A and Sample S

Sample	Particle density (kg/m^3)	Initial assembly height (mm)	Void ratio	Coordination number
A	2.70×10^6	154.220	0.683	4.351
S	7.85×10^6	150.640	0.644	4.401

observed at equilibrium. When gravitational force is applied, the distribution of the contact force between particles and the forces acting on the walls changes. The stress on the top of the prism is decreased. The system reaches another state of equilibrium.

In phase two, the particle friction coefficients of SA and SS are increased to 0.18 and 0.15, respectively. The system is allowed to reach a new state of equilibrium. Since the particles are packed in the prism, small stress (0.215 kPa for SA and 0.447 kPa for SS) still exists acting on the top wall of the prism. Then, the top wall is raised to a height of 1000 mm in the z-direction (see Fig. 7b). Releasing the stress at the top introduces particles rearrangement. The system is considered in equilibrium again when the unbalanced force ratio $\leqslant 1\,\%$. At this state, the stress at the bottom of the prism equals the normal pressure due to the weight of the spheres. In phase three, the particles are raised to the drop height (see Fig. 7c). The characteristics of the prepared samples of SA and SS before dropping are listed in Table 1.

3.3 Coefficient of restitution

For impact problems, the kinetic energy of the system is dissipated through mutual collisions between particles, which are usually modelled as damping. The restitution coefficient is defined as the ratio of the recoil velocity to the impact velocity, it reflects the energy dissipation during contact. The coefficient of restitution depends on many parameters, such as particle size (R), impact velocity (v_0), Young's modulus (E), and so on for each of the impacting particles [23]. Figure 8 shows the relation between the restitution coefficient and β. The restitution coefficient is determined by measuring the particle velocity before and after impact. The restitution coefficient for sphere-sphere impacts is about 19 % smaller than sphere-plate impacts. This is in agreement with the experimental results of steel, brass, aluminum, and Delrin spheres (20 %) by King et al. [13]. Therefore, the same β can be used to simulate particle and particle collision and particle and boundary collision. The coefficient of restitution decreases with the increase of β. Compared to SS, the restitution coefficient of SA is greater. It decreases slower with the increase of β which indicates that more kinetic energy of the system is dissipated in particle collision for SS. Thus β may have different physical meanings for different particles. However, the different restitution coefficient between SA and SS is minimal for $\beta \leqslant 0.01$.

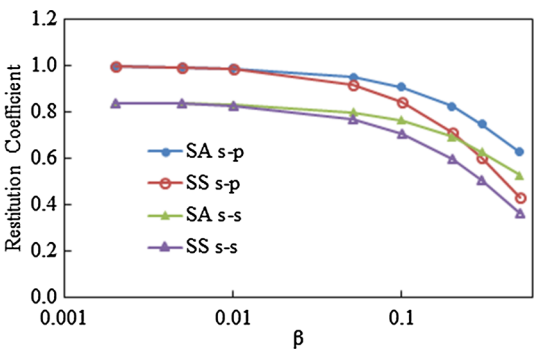

Fig. 8 Relationship between restitution coefficient and β (SA and SS are sample A and sample S, s-p and s-s are sphere-plate impact and sphere-sphere impact, respectively)

3.4 Numerical drop tests

Fifteen drop simulations have been conducted on Sample SA, as well as Sample SS, with five values of β (0.0005, 0.001, 0.002, 0.003, and 0.005) and three drop heights h_0 (225, 425 and 800 mm). These drop heights are the same as those of the physical experiments. Table 2 shows the test names of different β and h_0. The numbers and letters in the test names are used to distinguish different β and h_0 values. Particles are released from the drop height. Damping is applied during this dropping process when particles are in contact. The snapshots of test TA3b ($\beta = 0.002$ and $h_0 = 425$ mm) are shown in Fig. 9. When the support is removed, the particles at the bottom drop faster than those particles above. This is because of the downward contact force decreases with particle's elevation under gravity. Particles disperse during descending. Particles bounce upward after the collision with the bottom. The bouncing phenomenon becomes less obvious as damping increases. The unbalanced forces are also monitored. The deposition process is considered completed when the unbalanced force ratio is $<1\,\%$.

Table 2 β and h_0 used in numerical simulations

Sample	β	$h_0 = 225$mm	$h_0 = 425$mm	$h_0 = 800$mm
A	0.0005	TA1a	TA1b	TA1c
	0.001	TA2a	TA2b	TA2c
	0.002	TA3a	TA3b	TA3c
	0.003	TA4a	TA4b	TA4c
	0.005	TA5a	TA5b	TA5c
S	0.0005	TS1a	TS1b	TS1c
	0.001	TS2a	TS2b	TS2c
	0.002	TS3a	TS3b	TS3c
	0.003	TS4a	TS4b	TS4c
	0.005	TS5a	TS5b	TS5c

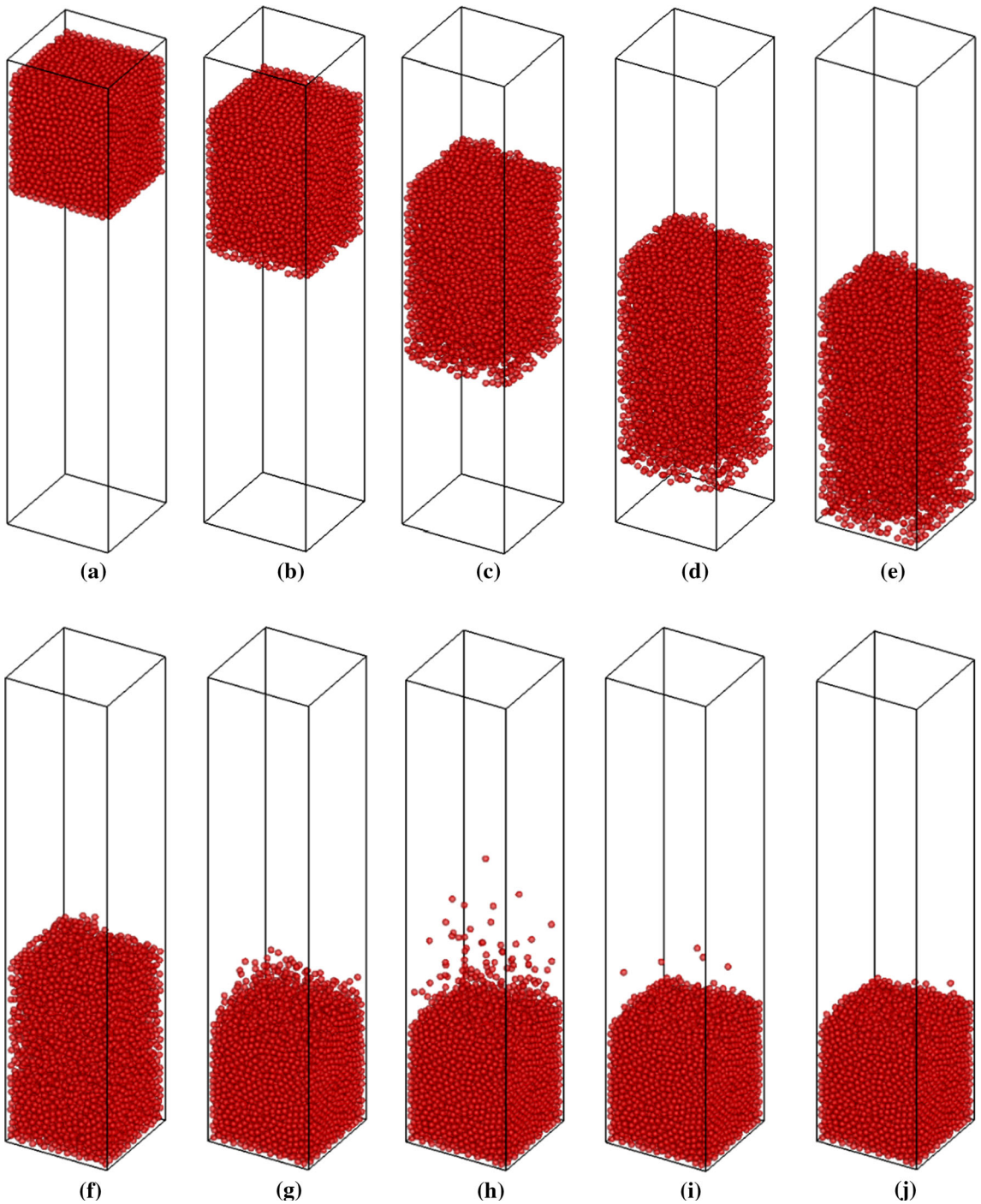

Fig. 9 Snapshots of test TA3b during dropping process: **a** t = 0s; **b** t = 0.126s; **c** t = 0.210s; **d** t = 0.269s; **e** t = 0.295s; **f** t = 0.320s; **g** t = 0.379s; **h** t = 0.463s; **i** t = 0.632s; **j** t = 0.800s

Figure 10 shows the relationship between h_0 and h_f with different β. The symbols are for the DEM simulations and the box charts are for the experimental tests. Since the surface of the numerical sample is not even, the average of the elevation of all particles at the top layer is reported. Figure 11 shows the projection of the positions of the particles at the top layer on the x, z plane. The solid line is the estimated average height for the test TA3b.

Comparing the numerical simulations with experimental tests, the results are similar for $\beta \geqslant 0.002$. $\beta \geqslant 0.005$ is not good for steel balls but it is still fine for aluminum balls. Therefore, DEM simulations ($0.002 \leqslant \beta \leqslant 0.003$) match experimental results better.

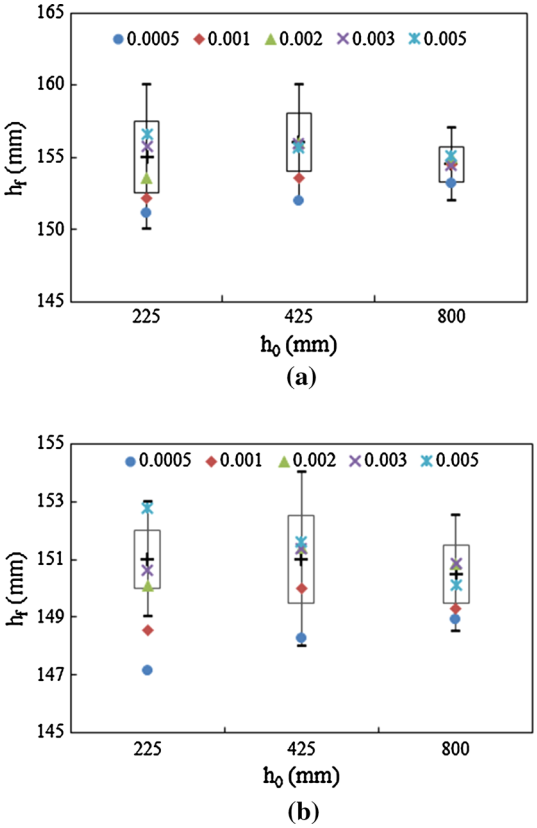

Fig. 10 Relationship between h_0 and h_f with different β. **a** Sample A. **b** Sample S

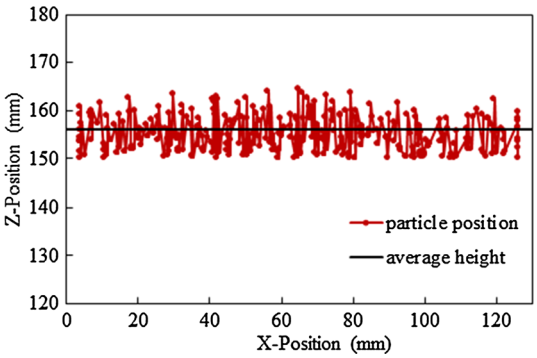

Fig. 11 The positions of particles at the top layer and the average height

4 Analysis

4.1 DEM simulations with additional h_0

Twenty-five additional DEM simulations have been conducted on SA and SS with another five h_0 (100, 150, 600, 1000 and 1200 mm) as listed in Table 3. Figure 12 shows the variation of h_f with h_0. The general trend among h_f, β and h_0 is similar for these two materials. h_f is a function of h_0, h_f first increases with the increase of h_0 to a maximum. Then h_f decreases slightly with further increase of h_0. The difference of h_f with various β is most obvious at $h_0 = 225$ mm. The difference among h_f decreases with the further increase of h_0. For low damping ($\beta = 0.0005$) or small h_0 ($\leqslant 225$ mm), h_f is significantly influenced by drop height. As β and h_0 increase, the influence of h_0 decreases. When β and h_0 are high ($\beta \geqslant 0.001$, $h_0 \geqslant 425$ mm), the kinetic energy of the system increases with increasing h_0. However, the increase of the kinetic energy cannot counter the energy lost in collisions. Therefore, there is no obvious increase in h_f.

Figure 13 shows the variation of h_f with different β. h_f is also a function of β. For $0.0005 \leqslant \beta \leqslant 0.002$ and all h_0, h_f of SA and SS both increase with the increase of β. This is in agreement with the findings of the previous numerical simulations [11]. Denser samples can be prepared with smaller β because lower damping in the simulation generates higher kinetic energy. For β between 0.002 and 0.005, h_f increases with β for $h_0 \leqslant 225$ mm while it various slightly for $h_0 \geqslant 425$ mm. The effect of damping is not significant when $\beta > 0.002$, $h_0 > 225$ mm. This indicates that the kinetic energy generated in the system may be almost the same for $\beta \geqslant 0.002$ when h_0 is greater than 225 mm.

4.2 Energy of the system

In order to analyze the effect of damping on the system during the dropping process of particles, the variation of the potential and kinetic energy of the system are monitored. Since similar behavior is observed for these two materials, the energy of SA is presented here only. Figure 14 shows the normalized potential energy of TA1a–TA5a and TA1g–TA5g with time (t). These energies are normalized with the initial values of TA1a. The potential energy decreases with time for both h_0 (225 and 1000 mm) until the system is in equilibrium. The potential energy of the system decreases slower as β increases. The effect of β is more obvious for a higher h_0. Figure 15 shows the normalized kinetic energy of TA1a–TA5a and TA1g–TA5g with time. The kinetic energy first increases to its maximum value and then decreases to a small value. Similar to the variation of potential energy, the kinetic energy also varies slower with the increase of β. The phenomenon is more obvious for a greater h_0. The maximum kinetic energy of the system occurs when some particles first touch the bottom. The maximum kinetic energy decreases with the increase of β. Less kinetic energy is generated in the system at this moment when a higher β is used during the free-falling process. Figure 16 shows the normalized total energy of TA1a–TA5a and TA1g–TA5g with time. The total energy first decreases slowly with time during the free-falling process. The energy decreases faster as β increases. Then, after the first particle reaches the bottom, the total energy decreases rapidly. The energy decreases slower as β increases. It takes more time for energy to dissipate during

Table 3 β and h_0 used in numerical simulations

Sample	β	h_0 = 100mm	h_0 = 150mm	h_0 = 600mm	h_0 = 1000mm	h_0 = 1200mm
A	0.0005	TA1d	TA1e	TA1f	TA1g	TA1h
	0.001	TA2d	TA2e	TA2f	TA2g	TA2h
	0.002	TA3d	TA3e	TA3f	TA3g	TA3h
	0.003	TA4d	TA4e	TA4f	TA4g	TA4h
	0.005	TA5d	TA5e	TA5f	TA5g	TA5h
S	0.0005	TS1d	TS1e	TS1f	TS1g	TS1h
	0.001	TS2d	TS2e	TS2f	TS2g	TS2h
	0.002	TS3d	TS3e	TS3f	TS3g	TS3h
	0.003	TS4d	TS4e	TS4f	TS4g	TS4h
	0.005	TS5d	TS5e	TS5f	TS5g	TS5h

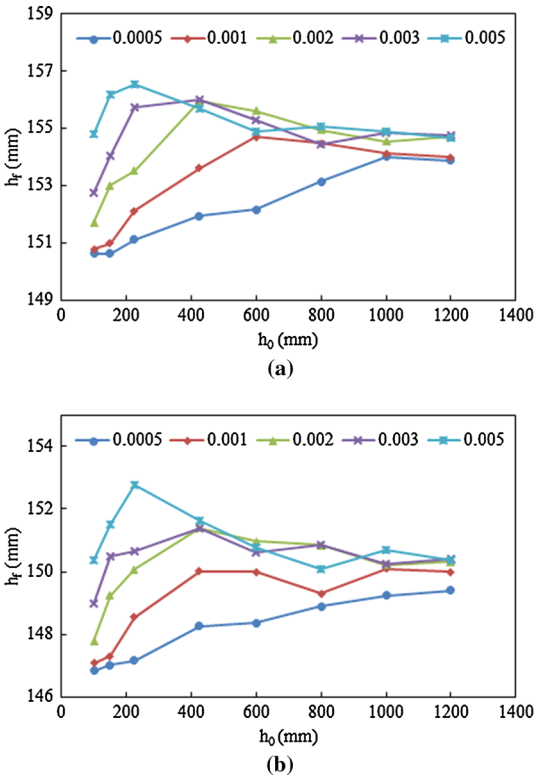

Fig. 12 Variation of h_f with different h_0. **a** Sample A. **b** Sample S

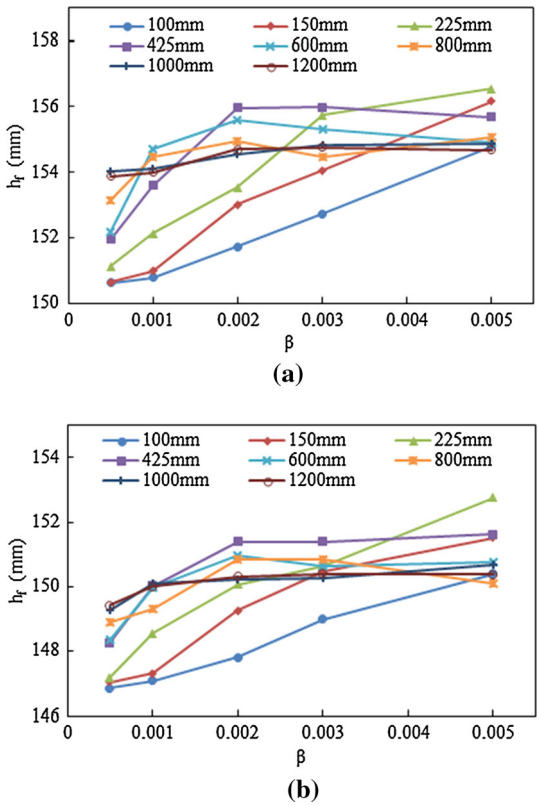

Fig. 13 Variation of h_f with different β. **a** Sample A. **b** Sample S

dropping when a higher β is used. The energy dissipation process slows down with the increase of β.

The particle dispersion during dropping is a function of β. Figure 17 shows the distribution of the particles when the first particle reaches the bottom of the prism for tests TA1a–TA5a (h_0 = 225 mm) and TA1g–TA5g (h_0 = 1000 mm). The influence of β on the degree of particle dispersion is evident. Particles disperse more with the increase of β. It reflects the effect of β in the variation of energy. As β increases, more energy is lost in particle collision. The phenomenon is more profound for tests TA1g–TA5g in which h_0 = 1000 mm. Figures 18 and 19 show the normalized potential and kinetic energies for all tests when the first particle reaches the bottom of the prism. These energies are normalized with the values of TA1a and TS1a for easy comparison. For both samples, the normalized kinetic energy decreases with β. When β increases, as particles disperse more (Fig. 17), the velocities of the particles at a higher elevation are smaller. Therefore, the distribution of particle velocities becomes less uniform so that less kinetic energy is developed. As h_0 increases, the effect of β becomes more obvious. A higher h_0 provides more time for particle free-falling and more space for particle dis-

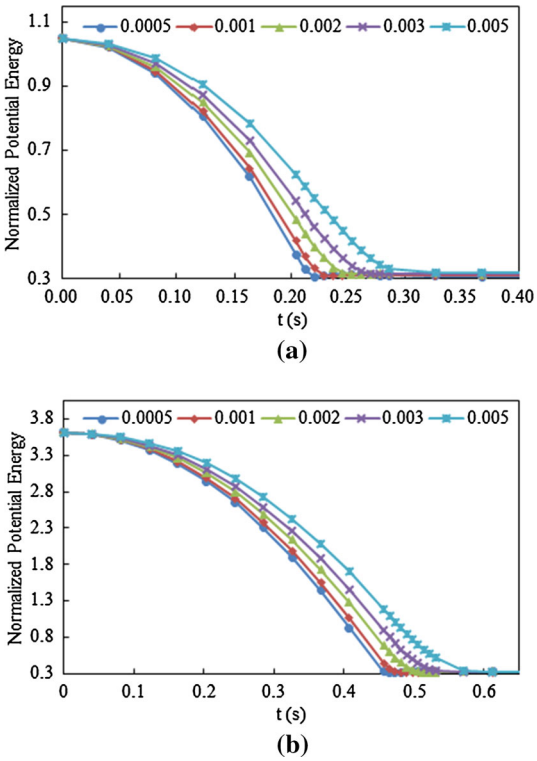

Fig. 14 Evolution of normalized potential energy with time. **a** TA1a–TA5a. **b** TA1g–TA5g

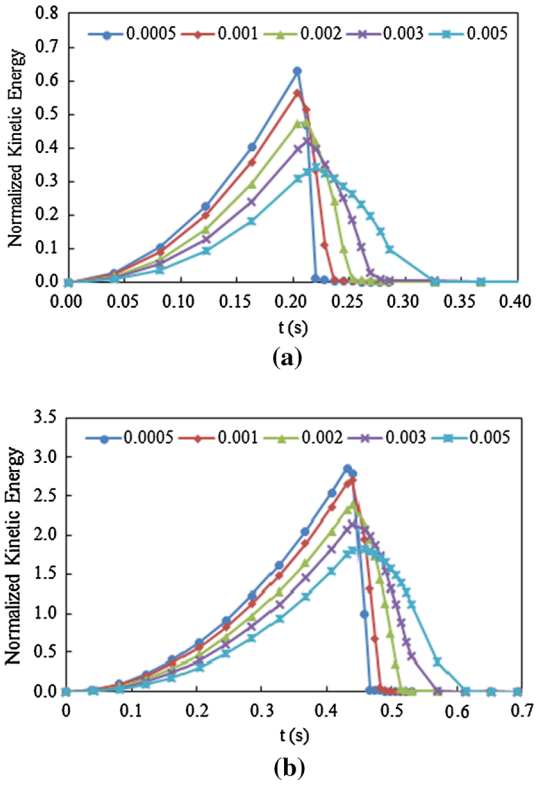

Fig. 15 Evolution of normalized kinetic energy with time. **a** TA1a–TA5a. **b** TA1g–TA5g

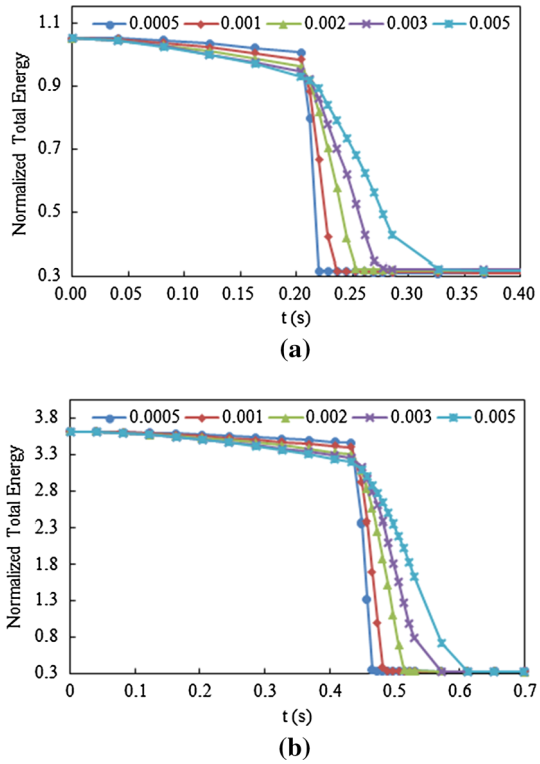

Fig. 16 Evolution of normalized total energy with time. **a** TA1a–TA5a. **b** TA1g–TA5g

persion. Thus a more obvious variation in the potential and kinetic energy can be observed.

4.3 Coordination number

The coordination number, C_n, is defined as the average number of contacts per particle. The evolution of C_n during the dropping process has been monitored. It can reflect the degree of collisions between particles. Figure 20 shows the evolution of C_n, the normalized potential, kinetic and total energy (E_p, E_k and E_t) of TA4a. The evolution can be divided into three stages (see Fig. 20) to distinguish the process before and after the first particle reaches the bottom and the particles finally adjust to equilibrium. In the free-falling part, C_n decreases very quickly before the first particle reaches the bottom. Very few collision occurs during this stage and the total energy of the system dissipates slowly. In the bouncing and settling stage, C_n increases rapidly after particles reach the bottom. The rate of the increase is less than that of the initial decrease of C_n. Collision between particles increases rapidly. Thus the kinetic energy decreases and so does the total energy. In the final adjustment stage, C_n increases slowly. New contacts continues to develop even the unbalanced force ratio is very small. Particles are adjusting to achieve the final static equilibrium.

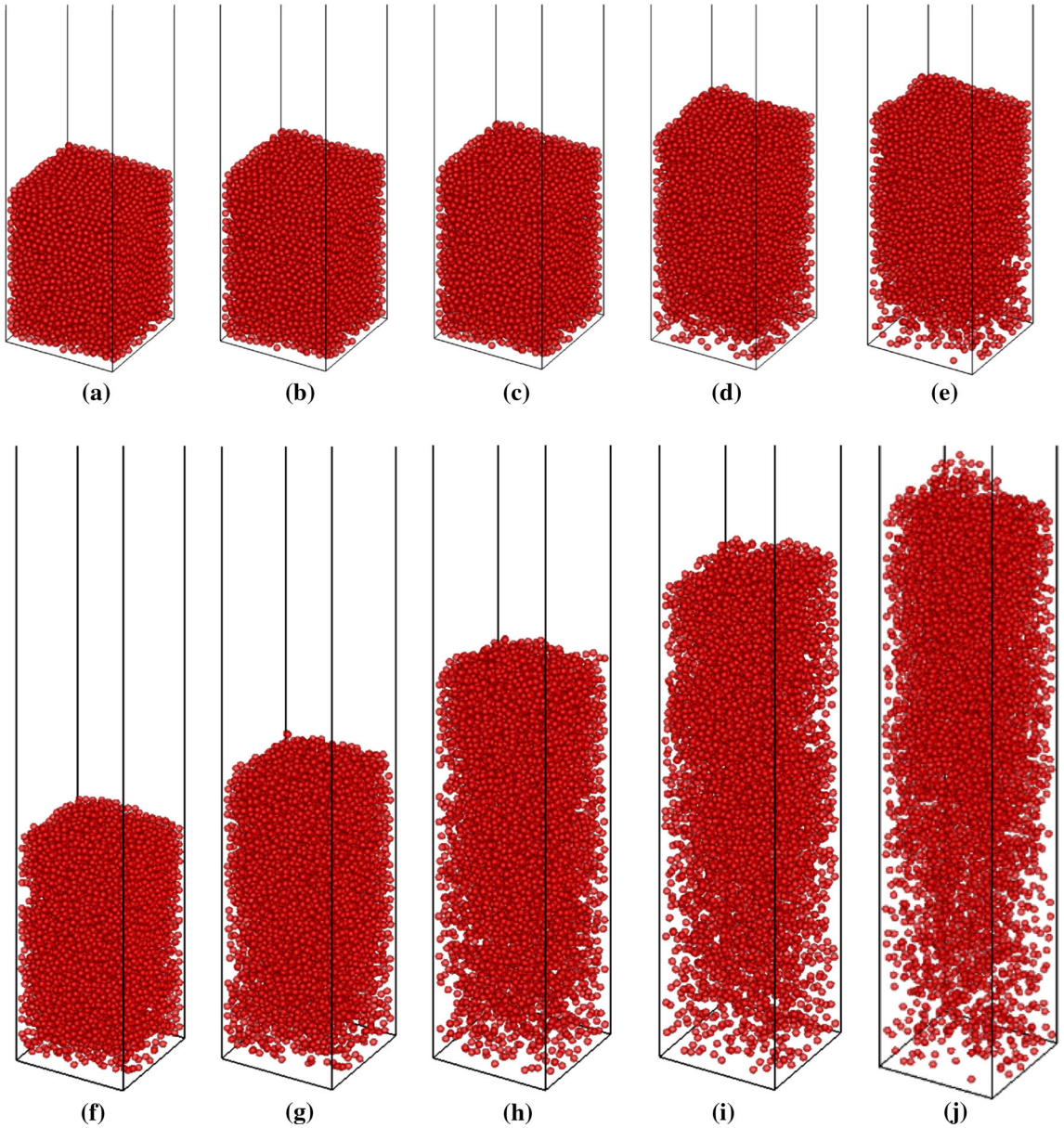

Fig. 17 Distribution of the particles when the lowest particles reach the bottom of the prism. **a** TA1a, **b** TA2a, **c** TA3a, **d** TA4a, **e** TA5a, **f** TA1g, **g** TA2g, **h** TA3g, **i** TA4g, **j** TA5g

The evolutions of C_n of TA1a–TA5a and TA1g–TA5g are shown in Fig. 21. Similar overall trend is observed. During the free-falling process, a greater C_n is obtained when a higher β is used. This indicates that collision between particles increases with the increase of β during free-falling. Thus the kinetic energy dissipates more as β increases (Fig. 19). Then, when the first particle reaches the bottom, C_n begins to increase until the equilibrium is reached. C_n increases faster as β increases during this process. More collisions occur when a higher β is used. This process takes more time for TA1g–TA5g because of the greater degree of dispersion (see Fig. 17).

5 Conclusions

Particle dropping tests have been carried out physically and numerically. 6000 particles have been released from a certain height and the process has been investigated. Three different drop heights and two kinds of metal particles have been used. Five different β have been used in DEM simulations to determine the appropriate β. Through comparing with experimental data, excellent agreement is found for the simulations using $0.002 \leqslant \beta \leqslant 0.003$. The determination process of β should be very good because of the high fidelity of DEM simulations to the physical tests.

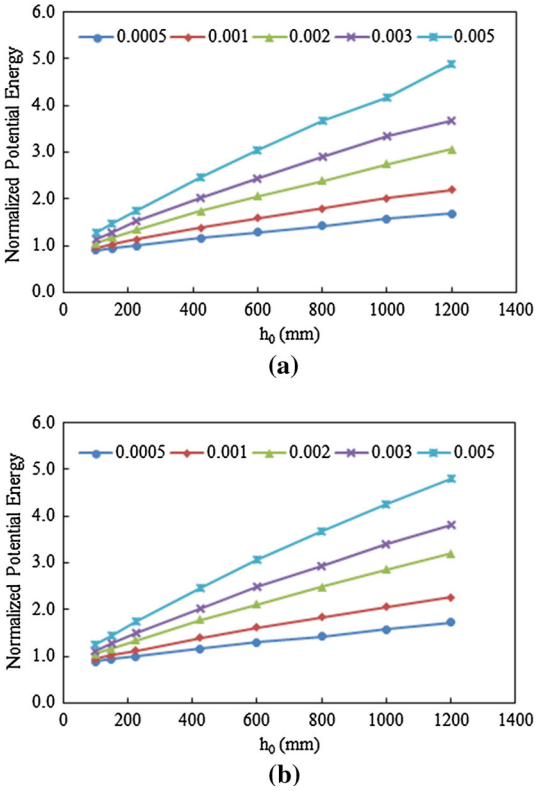

Fig. 18 Normalized potential energy when the first particle reaches the bottom of the prism. **a** Sample A. **b** Sample S

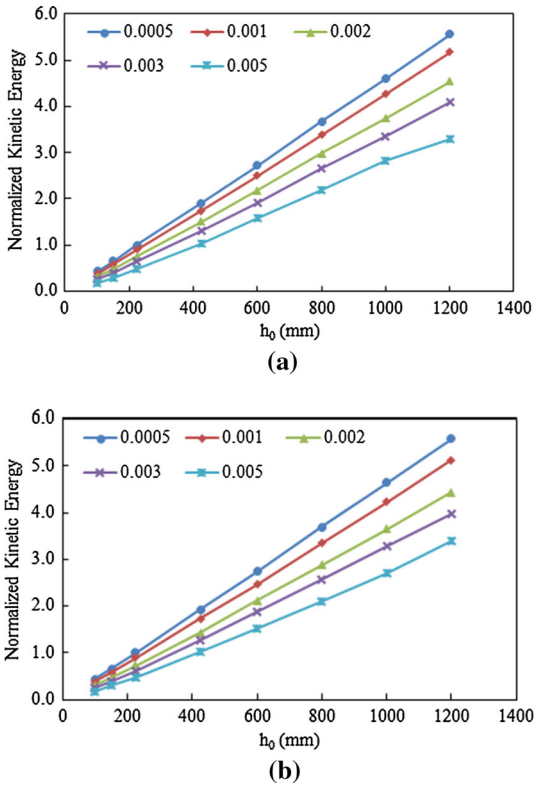

Fig. 19 Normalized kinetic energy when the first particle reaches the bottom of the prism. **a** Sample A. **b** Sample S

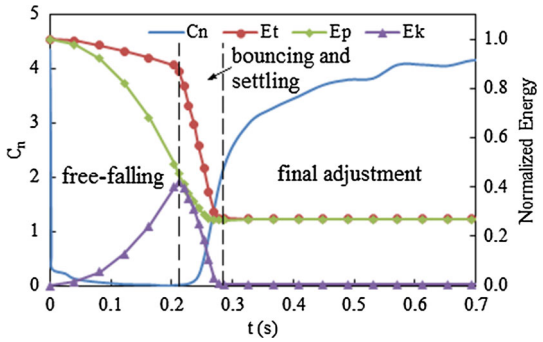

Fig. 20 Evolution of C_n, E_t, E_p and E_k

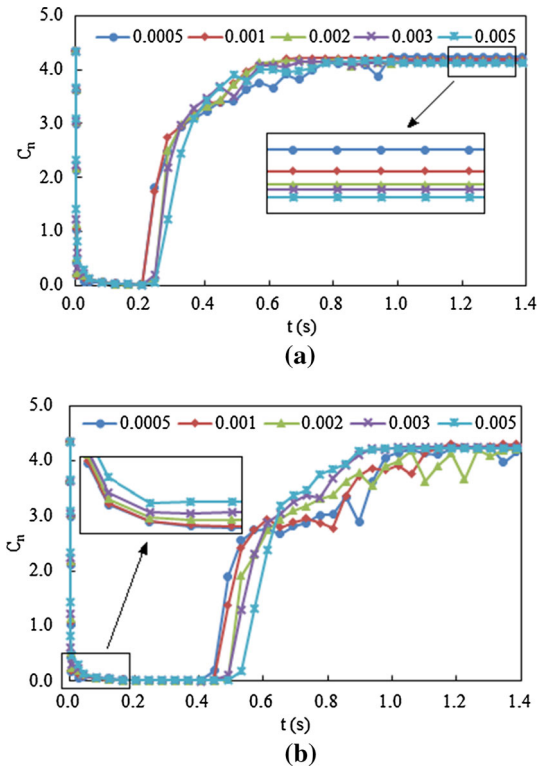

Fig. 21 Evolution of C_n with time. **a** TA1a–TA5a. **b** TA1g–TA5g

Additional numerical simulations have been conducted on SA and SS to further investigate the relationship between β, h_0 and h_f. The result shows that, h_f is a function of β and also a function of h_0. h_f increases with the increase of β for drop height $h_0 \leqslant 225$ mm. When h_0 increases from 425 to 800 mm, h_f increases with β for $0.0005 \leqslant \beta \leqslant 0.002$ and varies slightly for $0.002 < \beta \leqslant 0.005$. The effect of β is not significant when h_0 is higher than 1000 mm. For a certain β, h_f first increases with the increase of h_0 to a maximum and then decreases slightly with further increase of h_0. Evolution of the energies monitored during the simulations indicates that damping has an influence on the transformation between the potential and kinetic energy during the dropping process. Since the potential energy interacts with kinetic energy, it is

shown that the effect of damping is mainly due to the collision between particles.

Acknowledgments This work is partially supported by the National Natural Science Foundation of China (Grant Nos. 51379161 and 51322905).

References

1. Cundall, P.A., Strack, O.D.L.: The development of constitutive laws for soil using the distinct element method. Numer. Methods Geomech. **1**, 289–317 (1979)
2. Landry, H., Lague, C., Roberge, M.: Discrete element representation of manure products. Comput. Electron. Agric. **51**(1), 17–34 (2006)
3. Ng, T.T.: Input parameters of discrete element methods. J. Eng. Mech. **132**(7), 723–729 (2006)
4. Grima, A.P., Wypych, P.W.: Investigations into calibration for discrete element modelling of granular materials. In: Proceedings of the 6th International Conference for Conveying and Handling of Particulate Solids, Brisbane, Australia (2009)
5. Grima, A.P., Wypych, P.W.: Investigation into calibration of discrete element model parameters for scale-up and validation of particle-structure interactions under impact conditions. Powder Technol. **212**(1), 198–209 (2011)
6. Grima, A.P., Wypych, P.W.: Development and validation of calibration methods for discrete element modelling. Granul. Matter **13**(2), 127–132 (2011)
7. Zhang, D., Whiten, W.J.: The calculation of contact forces between particles using spring and damping models. Powder Technol. **88**(1), 59–64 (1996)
8. Grasselli, Y., Bossis, G., Goutallier, G.: Velocity-dependent restitution coefficient and granular cooling in microgravity. EPL Europhys. Lett. **86**(6), 60007 (2009)
9. Durda, D.D., Movshovitz, N., Richardson, D.C., Asphaugb, E., Morganb, A., Rawlingsd, A.R., Vestd, C.: Experimental determination of the coefficient of restitution for meter-scale granite spheres. Icarus **211**(1), 849–855 (2011)
10. Montaine, M., Heckel, M., Kruelle, C., Schwager, T., Pöschel, T.: Coefficient of restitution as a fluctuating quantity. Phys. Rev. E **84**(4), 041306 (2011)
11. Imre, B., Räbsamen, S., Springman, S.M.: A coefficient of restitution of rock materials. Comput. Geosci. **34**(4), 339–350 (2008)
12. Güttler, C., Heißelmann, D., Blum, J., Krijt, S.: Normal Collisions of Spheres: A literature survey on available experiments. arXiv:1204.0001 (2012)
13. King, H., White, R., Maxwell, I., Menon, N.: Inelastic impact of a sphere on a massive plane: nonmonotonic velocity-dependence of the restitution coefficient. EPL Europhys. Lett. **93**(1), 14002 (2011)
14. Mao, K., Wang, M.Y., Xu, Z., Chen, T.: DEM simulation of particle damping. Powder Technol. **142**(2), 154–165 (2004)
15. Fang, X., Tang, J., Luo, H.: Granular damping analysis using an improved discrete element approach. J. Sound Vib. **308**(1), 112–131 (2007)
16. Sun, Q., Jin, F., Zhou, G.G.D.: Energy characteristics of simple shear granular flows. Granul. Matter **15**(1), 119–128 (2013)
17. Bi, Z., Sun, Q., Jin, F., Zhang, M.: Numerical study on energy transformation in granular matter under biaxial compression. Granul. Matter **13**(4), 503–510 (2011)
18. Bridges, F.G., Supulver, K.D., Lin, D.N.C., Knightc, R., Zafrac, M.: Energy loss and sticking mechanisms in particle aggregation in planetesimal formation. Icarus **123**(2), 422–435 (1996)
19. Ng, T.T., Zhou, W., Ma, G., Chang, X.L.: Damping and particle mass in DEM simulations under gravity. J. Eng. Mech. **141**(6), 04014167 (2014)
20. Ng, T.T.: Triaxial test simulations with discrete element method and hydrostatic boundaries. J. Eng. Mech. **130**(10), 1188–1194 (2004)
21. Cundall, P.A., Strack, O.D.L.: A discrete numerical model for granular assemblies. Geotechnique **29**(1), 47–65 (1979)
22. Maeda, K., Hirabayashi, H.: Influence of grain properties on macro mechanical behaviours of granular media by DEM. J. Appl. Mech. **9**, 623–630 (2006)
23. Weir, G., Tallon, S.: The coefficient of restitution for normal incident, low velocity particle impacts. Chem. Eng. Sci. **60**(13), 3637–3647 (2005)